

**Rubber plant root properties induce contrasting soil aggregate stability
through cohesive force and reduced land degradation risk in southern China**

Waqar Ali¹, Amani Milinga¹, Tao Luo², Mohammad Nauman Khan³, Asad Shah³, Khurram
Shehzad⁵, Qiu Yang¹, Huai Yang⁴, Wenxing Long¹, Wenjie Liu^{1*}

¹*Center for Eco-Environment Restoration Engineering of Hainan Province, School of Ecology,
Hainan University, Haikou, 570228, China.*

²*CSIRO Agriculture and Food, Private Bag 5, Wembley, WA 6913, Australia.*

³*School of Breeding and Multiplication (Sanya Institute of Breeding and Multiplication), Hainan
University, Haikou, 570228, China*

⁴*Institute of Tropical Bamboo, Rattan & Flower, Sanya Research Base, International Center for
Bamboo and Rattan, Sanya 572000, China*

⁵*Hubei Key Laboratory of Soil Environment and Pollution Remediation, College of Resources and
Environment, Huazhong Agricultural University, Wuhan, 430070, China*

*** Corresponding authors: Wenjie Liu**

E-mail: liuwj@hainanu.edu.cn

Tel: 86-17733181789

Abstract

In southern China, Hainan Island faces land degradation risks due to a combination of soil physical, chemical, and climatic factors. Specifically, soil physical properties like a high proportion of microaggregates (<0.25 mm), chemical properties such as low soil organic matter (SOM) content, and a climatic factor of frequent uneven rainfall. The cohesive force between soil particles, which is influenced by plant root properties and root-derived SOM, is essential for improving soil aggregate stability and mitigating land degradation. However, the mechanisms by which rubber plant root properties and root-derived SOM affect soil aggregate stability through cohesive forces in tropical regions remain unclear. This study evaluated rubber plants of different ages to assess the effects of root properties and root-derived SOM on soil aggregate stability and cohesive forces. Older rubber plants (> 11 -years-old) showed greater root diameters (RD) ($0.81\text{--}0.91$ mm), higher root length (RL) densities ($1.83\text{--}2.70$ cm cm⁻³), and increased proportions of fine ($0.2\text{--}0.5$ mm) and medium ($0.5\text{--}1$ mm) roots, leading to higher SOM due to lower lignin and higher cellulose contents. Older plants exhibited higher soil cohesion, with significant correlations among root characteristics, SOM, and cohesive force, whereas the random forest (RF) model identified aggregates (> 0.25 mm), root properties, SOM, and cohesive force as the key factors influencing mean weight diameter (MWD) and geometric mean diameter (GMD). Furthermore, partial least squares-path models (PLS-PM) showed that the RL density (RLD) directly influenced SOM (path coefficient 0.70) and root-free cohesive force (RFCF) (path coefficient 0.30), which subsequently affected the MWD, with additional direct RLD effects on the SOM (path coefficient 0.45) and MWD (path coefficient 0.64) in the surface soil. Cohesive force in rubber plants of different ages increased macroaggregates (> 0.25 mm) and decreased microaggregates (< 0.25 mm), with topsoil average MWD following the order: Control (CK) (0.98 mm) $<$ 5Y_RF (1.26 mm) $<$ MF (1.31 mm)

< 11Y_RF (1.36 mm) < 27Y_RF (1.48 mm) < 20Y_RF (1.51 mm). Rubber plant root traits enhance soil aggregate stability and mitigate land degradation risk in tropical regions, offering practical soil restoration strategies through targeted root trait selection to strengthen soil cohesion, ensure long-term agricultural productivity, and preserve environmental quality, highlighting the need for further research across diverse ecological zones and forest types.

Keywords: Rubber plant root traits; soil organic matter; cohesive force; aggregate stability; land degradation

1. Introduction

Land degradation is a serious global issue that increases as a consequence of growing population and climate change, currently impacting > 75% of land and projected to affect > 90% by 2050 (Perović et al., 2021; Právělie et al., 2021; Thomas et al., 2023). Land degradation in tropical regions, such as Hainan Island, southern China, is driven by unfavorable soil conditions, including a high proportion of microaggregates (<0.25 mm) often observed in degraded soils due to macroaggregate breakdown which reduces structural stability, water infiltration, and low soil organic matter (SOM) content, which further weakens soil structure. Additionally, the uneven and high frequency of rainfall events during the summer season (May–October), combined with global climate change, further intensifies water erosion and accelerates land degradation (Shao et al., 2024; Zhu et al., 2022). In addition, zonal ferro-alumina lateritic soils (ferralsols) on Hainan Island, classified as having low resilience and sensitivity according to the tropical soil resilience-sensitivity matrix, are particularly prone to soil erosion (Li et al., 2022). Consequently, the current soil erosion area on Hainan Island has increased 4.8-fold compared to that in 2000, according to a third national soil erosion remote-sensing survey (Yu et al., 2016). Soil aggregates are fundamental to soil function, and their stability regulates carbon cycling, nutrient storage, soil fertility,

infiltration rate, and resistance to soil degradation (Hok et al., 2021; Rabot et al., 2018; Yudina and Kuzyakov, 2023). Therefore, it is imperative to enhance soil aggregate stability by implementing suitable management practices that protect the integrity of the environment and ensure sustainable agricultural productivity.

Natural rubber (*Hevea brasiliensis*) plantations have recently expanded rapidly across mainland Southeast Asia (Xu et al., 2023; Yang et al., 2024). Rubber plants are recognized for their effectiveness in improving soil aggregate stability through their root properties and in mitigating soil erosion (Kurmi et al., 2020; Sun et al., 2021). Root morphology, particularly traits like fine roots length (FRL), coarse roots length (CRL), root diameter (RD), and root length density (RLD), influences soil structure by enhancing particle binding. Fine roots, with their higher surface area, increase root-soil contact, promoting stronger aggregate formation through entanglement and cohesive force. Plant roots influence soil aggregate size distribution by promoting FRL, which closely interacts with soil particles, and negatively affecting CRL, which disintegrates into larger particles (Ali et al., 2022; Chen et al., 2021; Kumar et al., 2017). Plant morphological root traits, such as RD and RLD, and their chemical composition, including lignin and cellulose content, have been shown to alter carbon deposits in soil pools and their sequestration (Poirier et al., 2018b; Rossi et al., 2020). Nevertheless, several studies have suggested that the interaction between soil particles and plant root-derived SOM is limited, which significantly affects soil particle stability through cohesive forces, particularly after root decomposition (Ali et al., 2022; Chen et al., 2017). Variations in soil particles and root-derived SOM further adjust soil cohesion.

Soil cohesive forces, derived from SOM and the morphological and chemical properties of plant roots (Wang et al., 2018a; Wang et al., 2020), effectively stabilize sloped soils by enhancing soil-particle interactions, promoting flocculation, and minimizing soil erosion, thereby controlling

soil and water runoff (Smith et al., 2021; Wang et al., 2018a). Among these factors, SOM plays a complex role and is generally beneficial for promoting particle flocculation. However, an excess charge on SOM, combined with the negative charges of soil particles, can also lead to the dispersion of aggregates (He et al., 2021; Melo et al., 2021). The addition of plants and their roots allows for additional soil organic carbon (SOC) accumulation in the soil (Rossi et al., 2020). Roots can also bind soil particles via cohesive forces, thus increasing aggregate stability (Forster et al., 2022; Poirier et al., 2018a; Wang et al., 2020). Dominant root traits influence soil particles through cohesive forces, and their subsequent effects on soil aggregate stability remain unknown.

So far, few studies have investigated the impact of rubber plant roots on soil aggregation in the tropical region of Hainan Island (Sun et al., 2021; Zou et al., 2021), and there is a complete lack of research regarding the mechanisms related to rubber plant root morphological and chemical properties, root-derived SOM, and cohesive forces in aggregate formation. We hypothesized that rubber plantations of different stand ages would promote soil cohesive forces through root properties and SOM among soil particles, ultimately improving aggregate stability. This study aimed to: 1) investigate the impact of stand-age rubber plant root traits and root-derived SOM on aggregate properties, and 2) explore the interconnections between root morphological and chemical characteristics, SOM, cohesive forces, and soil aggregate stability. The findings of this research will contribute to better management practices in the tropical regions of Hainan Island, helping to mitigate land degradation issues by enhancing aggregate stability and overall environmental quality.

2. Materials and methods

2.1. Experimental site overview

The study was conducted on Hainan Island in Danzhou (19°4'3''–19°12'42''N, and 109°47'6''–110°1'2''E, 182–255 m above sea level). In the study area, the annual averages for temperature, precipitation, and solar radiation are 23.5°C, 1831 mm, and 4579 MJ·m⁻²·yr⁻¹, respectively. November–April of the following year is the dry season, whereas May–October is the rainy season. Rubber (*Hevea brasiliensis*) and areca (*Areca catechu* L.) are the two primary commercial crops in the experimental region. Prior to rubber plantation, the land was covered by tropical rainforest. According to the USA Soil Taxonomy System, the soil is classified as a laterite ferralsol (Schad, 2023). The soil in the rubber plantation was composed of 43.71% sand, 8.28% silt, and 48.01% clay. The basic physical and chemical characteristics of the samples are listed in Table. 1.

2.2. Experimental design

Rubber plantations with four different stand ages were selected from the field. The treatments included five-year-old rubber forests (5Y_RF), with 2018 rubber trees (clone PR-107) planted at the recommended density (3 × 7 m, 480 plants·ha⁻¹) and crown density 30 %; 11-year-old rubber forests (11Y_RF), with 2012 rubber trees (clone PR-107) planted at the recommended density (3 × 7 m, 431 plants·ha⁻¹) and crown density 90 %; 20-year-old rubber forests (20Y_RF), with 2003 rubber trees (clone PR-107) planted at the recommended density (3 × 7 m, 346 plants·ha⁻¹) and crown density 90 %; 27-year-old rubber forests (27Y_RF), with 1996 rubber trees (clone PR-107) planted at the recommended density (3 × 7 m, 300 plants·ha⁻¹) and crown density 90 %; and mixed forest (MF) and control (no forest plants) (CK). The MF treatment represents a mixed forest system consisting of cinnamon (*Cinnamomum verum*) trees (planted in 2014) intercropped with 20-year-old rubber (*Hevea brasiliensis*) trees. This treatment was included to assess the potential benefits of mixed-species plantations on soil aggregation and stability compared to monoculture rubber plantations. We established a randomized complete block design

with three replicates. We selected 18 plots (30×30 m) separated by a transitional zone. Rubber plants with different stand ages were selected based on similar topographies (slope and gradient) and management practices. Rubber plantation canopy heights were approximately 20 m. The rubber plant rotation duration was approximately 40 yr, and the first latex tappings in this region occurred when the trees were five- or six-years-old. Chemical fertilizers were applied at the initial rubber plantation development stage according to local conventional farming practices. Additional details regarding the rubber plantations at the experimental site can be found in the study by Sun et al. (2021).

2.3. Root morphological and chemical composition analysis

In January 2024, three replications per depth per forest plot of soil samples with roots were taken at soil depths of 0–20 and 20–40 cm, using cutting rings (200 cm^3). Using the methodology outlined by Chen et al. (2021), the following root features were measured: RD, root mass density (RMD), RLD, and root surface area density (RSD). The cutting ring cores were placed in nylon bags and taken to the laboratory, where they were submerged in water for an hour before being manually washed using 0.55-mm sieves to collect the roots. The roots were scanned using an Epson Perfection V800 photo scanner (© 2024 Epson America, Inc), and WinRHIZO Pro Version 2009c software was used to assess the RD and RL. By dividing the entire RL and root surface area by the cutting-ring volume (cm^3), respectively, the RLD and RSD were calculated. The roots were oven-dried at 50°C , and the RMD was calculated by dividing the dry root mass by the cutting-ring volume. Furthermore, using data from the WinRHIZO analyzer, the root system was classified into four types based on RD: $\text{RD} < 0.2 \text{ mm}$ (very fine roots (VFRL)), $\text{RD} 0.2\text{--}0.5 \text{ mm}$ (fine roots (FRL)), $\text{RD} 0.5\text{--}1 \text{ mm}$ (medium roots (MRL)), and $\text{RD} > 1 \text{ mm}$ (CRL).

Chemical composition (cellulose and lignin) analysis of the roots was performed on three subsamples of the root classes ($RD < 0.5$, $0.5-1$, and > 1 mm). Briefly, 1 mg of 65 °C oven-dried root powder (< 0.5 mm) was mixed with 5 ml acetic acid and heated for 25 min, followed by three deionized water washings and supernatant discarding. Subsequently, 10 ml of sulfuric acid (10%) and 10 ml of potassium dichromic (0.1 mol L^{-1}) solutions were added, vortexed, and heated in a 100 °C water bath for 10 min. After cooling, 5 ml KI solution (20%) and 1 ml starch (0.5%) were added, shaken for 10 min, and then titrated with 0.2 mol L^{-1} sodium thiosulfate to determine cellulose and lignin contents (Zhang et al., 2014).

2.4. Soil cohesive force determination

Soil samples of approximately 2000 g were collected from depths of 0–20 cm and 20–40 cm using a soil auger during the root collection process. The samples were carefully extracted, combined, and sealed in plastic bags for transportation to the laboratory for further analysis. Soil samples were air-dried and divided into two parts. One part was ground to 100 μm for SOM determination using the oxidation method described by Walkley and Black (1934). The second part was dry-sieved to retain aggregates < 5 mm, and visible roots were removed. These soil samples were stored for subsequent analysis of the remolded soil root-free cohesion force (RFCF), which was determined according to the method described by Huang et al. (2022). Briefly, four subsamples for root soil composite cohesive force (RSCCF) were collected from each depth in three replicated plots using cutting rings (diameter = 10 cm, height = 6.37 cm) simultaneously during the root collection described in Section 2.3. These intact cores were used to determine soil cohesive forces. Soil cohesive force (c) was measured by assessing soil shear strength (τ) and vertical load (σ) applied to the shear surface, and c was calculated using the relationship between τ , σ , and c as described in Equation 1. In addition, soil (< 5 mm) without visible roots was remolded

into cutting rings (diameter = 10 cm, height = 6.37 cm) according to the soil bulk density (Table 1) at each soil depth in the rubber plots to measure the soil RFCF. In total, 48 core soil samples per treatment were used for soil cohesive force analysis. Both the RFCF and RSCCF samples were saturated with deionized water. After saturation, four subsamples from each depth and treatment were tested using an LH-DS-4 direct shear tester (Nanjing Technology Co., Ltd.), which has a shear strain accuracy of 0.01 mm and a shear stress accuracy of 0.01 N. The shear tester comprised a shear box, a sensor, a vertical compression device, and a displacement measurement system with specifications of 61.8 mm in diameter and a height of 20 mm. For the direct shear tests, four predetermined vertical loads (25, 50, 75, and 100 kPa) were applied. The shear rate of displacement was set at 0.8 mm min⁻¹, and the soils were sheared until failure, indicated by reaching the peak τ value on the computer. The relationship between the peak τ values and vertical loads (σ) was established according to Mohr–Coulomb’s law, and soil cohesion (c) was calculated as described in Equation 1.

$$\tau = c + \sigma \tan \varphi \quad (1)$$

where τ is the soil shear strength (kPa), σ is the vertical load applied to the shear surface (kPa), c is the soil cohesive force (kPa), and φ is the soil internal friction angle (°).

2.5. Soil aggregate analysis

Soil samples from depths of 0–20 and 20–40 cm were collected in each treatment simultaneously with the root sample collection. The soil was allowed to air dry and then gently ruptured along its natural cracks before it was passed through an 8 mm mesh sieve to determine the soil aggregate size distribution and stability. We used a wet sieving method to separate aggregates < 8 mm into four size groups: large macroaggregates (LMA) (> 2 mm); macroaggregates (MA) (2–0.25 mm); microaggregates (MIA) (0.25–0.053 mm); and small

microaggregates (SMA) (< 0.053 mm). Briefly, three replicates of 100 g of soil were immersed in deionized water for 10 min in a beaker before being transferred to a series of sieves with decreasing mesh sizes (2, 0.25, and 0.053 mm) and gently shaken in water with a 4-cm vertical vibration amplitude for 10 min. Subsequently, the soil that remained after each sieve was washed and transferred to a beaker, and all aggregate sizes (> 2, 2–0.25, and 0.25–0.053 mm) were oven-dried for 48 hours at 60 °C before being weighed. The mass of aggregates < 0.053 mm was determined by subtracting the total soil mass from the total mass of other aggregate sizes (Elliott, 1986). Equations 2 and 3 were used to compute the mean weight diameter (MWD, mm and geometric mean diameter (GMD), respectively (Kemper and Rosenau, 2018).

$$MWD = \sum_{i=1}^n W_i * X_i \quad (2)$$

where X_i denotes the mean diameter of aggregate fraction i, and W_i denotes the mass proportion of aggregate fraction i.

$$GMD = \exp \left[\sum_{i=1}^n W_i * \ln (X_i) \right] \quad (3)$$

where W_i represents the aggregate fraction mass proportion i, and X_i represents the mean diameter of aggregate fraction i.

2.6. Statistical analysis

Shapiro–Wilk ($p > 0.05$) and Levene's tests ($p > 0.05$) (Razali and Wah, 2011) were used to evaluate the normality and homogeneity of variances using SPSS 25 (IBM Corp., Chicago, USA). Origin 2021 software was used to evaluate each index. One-way analysis of variance (ANOVA) was conducted to determine statistical significance at $p < 0.05$, followed by Tukey's

test to assess treatment significance. Pearson's correlations among root characteristics, SOM, soil aggregate parameters, and soil cohesive force were assessed using Origin software (OriginLab Corp.). The random forest (RF) model was constructed using the R software Random Forest package (v4.3.1) (Team, 2017), with hyperparameters, including ntree, mtry, importance, proximity, etc., to optimize through grid search and 5-fold cross-validation. The Gini index assessed variable importance, and model performance was evaluated using MSE and R^2 on a 30% validation dataset. The partial least squares-path models (PLS-PM) were performed in R software (v4.3.1) using the "plspm" package to elucidate the bootstrapping (5,000 iterations) determined significance of path coefficients ($*p* < 0.05$, 95% CIs). The R^2 and bootstrapped p-values validated model adequacy through which plant root characteristics, SOM, and soil cohesive forces influence soil aggregate stability. Figures were created using Origin 2021 (OriginLab Corp.).

3. Results

3.1. Root distribution and chemical composition

Significant differences in root morphological traits were observed among rubber plantations of different stand ages (Fig. 1). The RD varied notably with the age of the rubber plant (Fig. 1a). The largest RD was found in 27Y_RF, followed by the MF at depths of 0–20 cm and 20–40 cm, respectively. Specifically, the largest RD for 27Y_RF was 0.84 mm and 0.91 mm at depths of 0–20 cm and 20–40 cm, respectively. By contrast, the smallest RD, found in five-year-old rubber plantations (5Y_RF), ranged from 0.42 to 0.45 mm across both depths, respectively. The differences in RD among rubber plants of varying stand ages depended on soil depth, with the most significant differences found at the 0–20 cm depth. Furthermore, there were notable variations in RLD between rubber plantations of different stand ages, as shown in Fig. 1b. The 27Y_RF exhibited the highest RLD, ranging from 1.83 to 2.81 cm cm^{-3} , followed by MF (2.01–

2.06 cm cm⁻³) and 20Y_RF (1.93–2.70 cm cm⁻³) at both depths. The RLD differences among rubber plants of various stand ages were influenced by soil depth, with the most noticeable differences occurring at a depth of 0–20 cm. In addition, the RSD and RMD were significantly different among rubber plantations of different stand ages (Fig. 1c, and d). Furthermore, RD distribution, represented as a percentage of RL within each RD class, also differed among rubber plantations of various stand ages (Fig. 2). In the 5Y_RF, 11Y_RF, and MF plantations, VFRL (< 0.2 mm) predominated at both soil depths. Conversely, in the 20Y_RF and 27Y_RF plantations, the roots were uniformly distributed across the soil depths, with a relatively high percentage of MRL (0.5–1 mm).

The root chemical composition varied among rubber plantations of different stand ages and RD classes (Fig. 3). The cellulose contents in stand-age rubber plants were significantly different (Fig. 3a). The 20Y_RF roots had higher cellulose content than those of the 27Y_RF, followed by the 11Y_RF. Similarly, cellulose content varied across the RD classes, with the 5Y_RF having lower cellulose levels than other stand-age rubber plants for FRL (< 0.5 mm). Moreover, there were significant differences in lignin content among the stand-age rubber plants and between the RD classes (Fig. 3b). For example, the lignin contents in the 20Y_RF were less than that in the 5Y_RF for RL < 0.5 mm. Cellulose and lignin contents are indicators of root contribution to SOM. Thus, the lower lignin and higher cellulose content in the 20Y_RF resulted in the highest SOM content ranging from 21.16 to 23.37 g kg⁻¹, followed by that in the 11Y_RF, ranging from 20.56 to 22.68 g kg⁻¹, and the 27Y_RF ranging from 21.04 to 21.78 g/kg within soil depth (Fig. 3c).

3.2. Soil cohesive force under different stand-age rubber plantations

There was a significant difference in the RFCF among rubber plantations of different stand ages (Fig. 4a). The CK (without plants) RFCF was 17.92 and 20.25 kPa at depths of 0–20 and 20–

40 cm, respectively, and the RFCF matrix significantly increased with the introduction of rubber plantations of different stand ages. For example, at 0–10 cm soil depth, compared to the CK, the ability of rubber plants to improve the soil cohesive force followed the order MF > 27Y_RF > 20Y_RF > 11Y_RF > 5Y_RF. For the 20Y_RF, the increases in RFCFs relative to the CK were 169.73 and 156 % at 0–20 and 20–40 cm, respectively. Generally, older rubber plants (> 11-years-old) yielded a greater RFCF than younger rubber plants.

The root–soil composite cohesive force exhibited different patterns among rubber plantations of different stand ages compared to that of the RFCF (Fig. 4b). The root–soil composite cohesive force showed significant differences among rubber plantations of different stand ages and with that in the CK at 0–20 cm depths, whereas the root–soil composite force was significantly greater with plants than with that in the CK at 20–40 cm depth. However, there were no significant differences in the root–soil composite cohesive forces among the different plantations within the 20–40 cm soil depth. This is likely because rubber plants of different stand ages (20Y_RF, 27Y_RF, and MF) had greater root–soil interactions, likely due to thicker RD, higher RLD, higher percentage of MRL, and higher SOM at a depth of 0–20 cm. Overall, both cohesive forces were significantly correlated with RLD, VFRL, FRL, and SOM (Fig. 6). These results indicate that rubber plantations of different stand ages have a greater ability to improve soil cohesive forces.

3.3. Soil aggregate properties under different stand-age rubber plantations

Soil aggregate properties exhibited different patterns among the various rubber plant treatments (Fig. 5). Soil aggregates sizes were predominantly 2–0.25 mm, followed by > 2 mm, and 0.25–0.053 mm, and aggregate sizes > 0.053 mm were less dominant in all rubber plantations of different stand ages compared to that in the CK at the respective soil depths (Fig. 5a–f). In the CK, the 2–0.025 mm aggregates accounted for 23.76% at a depth of 0–20 cm and 26.84% at 20–

40 cm. Compared to the CK, rubber plantations of different stand ages showed a significant increase in 2–0.25 mm aggregates at both soil depths. However, the proportion of aggregates > 2 mm, significantly increased in rubber plantations of different stand ages compared to that in the CK at respective soil depths, in the order 20Y_RF > 11Y_RF > 27Y_RF > MF > 5Y_RF. Simultaneously, the proportion of aggregates < 0.053 mm was significantly reduced in rubber plantations of different stand ages compared with the CK. The increase in macroaggregates (> 2 mm) and decrease in microaggregates (< 0.053 mm) following rubber plantation treatments of varying stand ages led to improvements in aggregate stability (measured by MWD and GMD) in the following order: 20Y_RF > 27Y_RF > 11Y_RF > MF > 5Y_RF > CK.

3.4 Relationship among root traits, SOM, cohesive force, and soil aggregate stability

The Pearson correlation analysis revealed a strong positive correlation between soil RFCF and MWD as well as GMD, with correlation coefficients of 0.81 and 0.91 (0–20 cm) and 0.81 and 0.89 (20–40 cm). In contrast, soil RFCF showed a significant negative correlation with small microaggregates (< 0.053 mm), with correlation values of –0.74 and –0.79 at both depths (Fig. 6). A similar pattern was observed for the root–soil composite cohesive force. In general, a stronger cohesive force was associated with higher RLD, greater proportions of FRL and MRL, and higher SOM, especially in older rubber plants, which contributed to their ability to maintain greater aggregate stability.

The Random Forest (RF) model highlighted the significance of various soil factors in predicting soil aggregate stability (MWD and GMD) across both soil depths (Fig. 7), with LMA (>2 mm) and MA (2–0.25 mm) emerging as the most influential contributors to stability, followed by SOM and FRL (FRL_0.2–0.5 mm). Root properties and soil cohesive forces also play substantial roles, particularly at deeper soil depths (20–40 cm), where cohesive forces become

more prominent. Furthermore, the PLS-PM clarified both the direct and indirect effects of root properties, SOM, and cohesive forces on soil aggregate stability (Fig. 8). Among the factors measured in the surface soil (0–20 cm), RLD (path coefficient 0.64, $P < 0.05$) directly influenced SOM (path coefficient 0.45, $P < 0.05$) and the MWD. In addition, RLD had a strong direct effect on SOM (path coefficient 0.70, $P < 0.05$). Furthermore, RLD directly altered RFCF (path coefficient 0.30, $P < 0.05$), which further affected the MWD. In contrast, RLD directly influenced the RSCCF, however, the RSCCF did not directly influence the MWD. A similar trend was observed in the deep soil (20–40 cm).

4. Discussion

4.1. Stand-age rubber plant roots influence on soil cohesive forces

Rubber plantations of different stand ages exhibited different root morphological traits. Our results demonstrated that the plant roots of rubber plantations aged < 11 -years-old were influenced by soil properties at 0–20 and 20–40 cm depths, as indicated by a sharp decline in RD and RLD (Fig. 1), and restricted root growth due to an increase in soil bulk density and a decrease in macropores. Similarly, Sun et al. (2021) observed that at the same research site, older rubber plants (13-years-old) exhibited a preference for growing in macropores compared to younger plants (four-years-old), which was attributed to their superior root properties and lower soil bulk density. In contrast, the 27Y_RF and MF were minimally influenced by soil properties due to the high percentage of FRL and MRL, which likely enlarged medium soil pores and facilitated penetration through capillary soil pores ($< 30 \mu\text{m}$) (Ali et al., 2022; Chen et al., 2021; He et al., 2022). Older rubber plants possess a higher proportion of FRL and MRL and produce a greater amount of root exudates, which likely function as lubricants to facilitate root growth in compacted soils with a higher bulk density (Chen et al., 2017; Sun et al., 2023). In our study, older rubber

plants demonstrated a higher root penetration ability than younger plants, which likely modified the soil cohesive forces.

Our results indicate that rubber plant roots of different stand ages were more effective in enhancing soil cohesive forces in tropical regions than in the CK (no rubber plants) (Fig. 4). Many studies have highlighted that plant roots enhance soil detachment resistance during rainfall events, primarily by increasing soil cohesive forces (Huang et al., 2022; Shen et al., 2021). Our findings further confirm that rubber plantations of different stand ages generate varying soil cohesive forces, which are influenced by their root properties and contributions to SOM. The differences in the enhancement of root–soil composite cohesive forces among rubber plantations of varying stand ages were attributed to their distinct root properties. Younger rubber plants (< 20Y_RF) were more effective at increasing soil cohesion in the topsoil (0–20 cm), whereas older plants improved soil cohesion in both the topsoil and deeper layers compared to that in the CK (Fig. 4) because of their higher root tensile strength, soil shear strength, and greater RD and RLD. However, the RD and RLD of younger plants were significantly reduced in the subsoil, thereby diminishing their impact on soil cohesion. In contrast, older rubber plants enhance soil cohesive forces because of their extensive root contact area with the soil and the high density of their crisscrossing FRL and MRL networks, which effectively bind and wrap soil particles (Huang et al., 2022; Vannoppen et al., 2015; 2017). In the current study, RLD and a substantial proportion of FRL and MRL in older rubber plants enhanced root–soil contact and strengthened the soil at both depths (Figs. 1, and 2).

The impact of roots on the cohesive force of root-free soils can be attributed to their indirect contribution to SOM. Soils from older rubber plantations, which exhibited higher SOM content (Fig. 3c), enhanced clay particle cohesion by reducing the surface tension of water within the clay–organic matter matrix (Wuddivira et al., 2009). RD and chemical composition (cellulose) altered

carbon sequestration in various soil pools, enhancing carbon accumulation in the coarse silt fraction (20–50 μm), while decreasing carbon accumulation in particulate organic matter (Liao et al., 2023; Zhang et al., 2014). Similarly, roots with higher cellulose-to-lignin ratios improve substrate availability for polymer-hydrolyzing enzymes, thereby speeding up the degradation of plant organic materials (Barto et al., 2010; Halder et al., 2021; Zhang et al., 2014). In addition, root exudates facilitate root penetration into compacted soil layers and increase the distribution frequency of SOM in deeper soil horizons (Oleghe et al., 2017). In general, older rubber plants exhibited a greater RLD, higher percentage of FRL and MRL, and increased SOM than younger rubber plants, which led to a higher RFCF.

4.2. Aggregate stability responses to soil cohesive forces under different stand-age rubber plantations

Our study provides comprehensive insights into soil aggregate stability across rubber plantations at different stages of stand maturity. Soil cohesive forces driven by plant root traits are key factors in enhancing soil aggregate stability. The soil cohesive force increased aggregate stability (MWD and GMD) at the same soil depth (Fig. 5). The root morphology traits like fine FRL, CRL, RD, RLD, influence the soil cohesive force and binding of soil particles and then indirectly increase aggregate stability (MWD and GMD). The results also indicated that cohesive forces not only governed macroaggregate stability but also played a role in microaggregate formation. Macroaggregates are primarily stabilized by cohesive forces derived from organic matter, root exudates, and fungal hyphae. In our study, the significant increase in RFCF with the introduction of rubber plantations (Fig. 4a) indicates that cohesive forces are enhanced by root activity and organic matter inputs. Similarly, microaggregates are formed through the binding of primary particles (clay, silt, and fine organic matter) by cohesive forces. In our study, the increased RFCF in older plantations (Fig. 4a) suggests that cohesive forces are strong enough to facilitate

the formation of microaggregates, particularly in the topsoil (0–20 cm depth). The MWD increased across rubber plantations of different stand ages because of the significant enhancement in soil cohesive forces. Rubber plants older than 11 years exhibited the highest aggregate stability at the same soil depth, which was consistent with the trend observed in their RFCF (Fig. 4). High soil cohesion has also been documented to limit soil dispersion rates and mitigate gully erosion (Wuddivira et al., 2013). Although the soil RFCCF was highest in older rubber plantations, the highest SOM content likely played a positive role in stabilizing soil particles (Kamau et al., 2020). SOM influences soil particles in several ways, primarily by enhancing soil aggregation and improving soil structure. SOM contributes to the formation of aggregates by acting as a binding agent between soil particles, especially through its interaction with clay minerals and other soil constituents. The organic compounds in SOM help form cohesive forces that promote the flocculation of fine soil particles, creating larger, more stable aggregates. SOM had a positive effect on soil particles as its dispersive properties became evident only once the soil aggregates were broken down. High SOM content also weakens the electrostatic repulsive forces by influencing the overlap of oppositely charged electric double layers (Ali et al., 2023; Yu et al., 2020). In addition, the higher MWD observed in rubber plantations older than 11 years, compared to those in the 5Y_RF and CK, indicated that the MWD of older rubber plants was not adversely affected by the excessive release of SOC from the mechanical breakdown of macroaggregates. During this breakdown process, the enhanced root biomass and higher SOM content in older rubber plantations help stabilize soil aggregates and mitigate the adverse effects of SOC loss. Additionally, higher RLD and root-derived SOM in older plantations promote microaggregate formation, further supporting aggregate stability and contributing to the observed increase in MWD, despite the release of some SOC from macroaggregate breakdown.

These findings highlight the importance of understanding the specific mechanisms by which soil cohesive forces contribute to aggregate stability. In this study, the soil aggregate portion (< 0.25 mm) was comparatively higher in the rubber plantations than in the control in this study. Rubber plant roots and SOM positively enhanced cohesion between soil particles (Fig. 5a–f). The soil cohesive force regulates soil aggregate stability using the following approaches. First, smaller aggregates, due to their higher surface area to volume ratio with water, can create surface tension between particles, indirectly creating a cohesive force, helping to hold them together (Wang et al., 2023). Second, soil particles, particularly clay and organic matter, often carry electrical charges that can lead to electrostatic attraction, further stabilizing the soil particles (Kaiser and Asefaw, 2014; Wuddivira et al., 2009). SOM has a positive effect on clays because the dispersive effect of SOM is not expressed until the aggregates are broken (Melo et al., 2021). High SOM also weakens the electrostatic repulsive force in ultisols through its additional impact on the overlap of oppositely charged electric double layers (Ali et al., 2023; He et al., 2021; Yu et al., 2020). Third, the water in the small pores between the soil particles creates a capillary force that contributes to the soil cohesive force, which agglomerates the small particles (Deviren Saygin et al., 2021). In general, stand-age rubber plantations positively improved soil aggregate stability compared to the control through soil cohesion. In young rubber plantations, legumes such as kudzu should be planted. Furthermore, the development of a forest rubber understory economy can significantly enhance soil health by increasing biodiversity, with diverse plant roots improving soil structure, promoting microbial activity, preventing erosion, and contributing to organic matter through leaf litter and root biomass, thereby improving soil fertility. Future research should focus on evaluating the mechanisms by which various understory plants in rubber plantations reduce soil erosion.

5. Conclusion

In this study, we investigated how root morphological traits, root-derived SOM, and the chemical composition of rubber plants at different stand ages influence soil aggregate stability through soil cohesive forces. Our findings indicate that natural rubber plantations of different stand ages exhibit distinct root distribution patterns, with older rubber plantations, particularly 27-year-old rubber forests, and MF demonstrating a more developed root system characterized by greater RLD and higher proportions of FRL and MRL diameter classes compared to younger plantations. The higher percentages of FRL and MRL in older rubber plants (> 11 years old), along with their high SOM content, contributed to a stronger soil cohesive force than that observed in younger rubber plants and the control plots. The higher SOM content in older rubber plants was driven by the higher cellulose content and lower lignin percentages in their FRL and MRL. Consequently, rubber plants older than 11 years increased the soil cohesive force (with and without roots) compared to younger rubber plants and the control, thereby enhancing aggregate stability and reducing soil particle dispersion. These findings offer practical implications for managing rubber plantations across different stand ages to restore soil quality in degraded tropical regions of Hainan Island. For instance, younger stands may benefit from targeted organic amendments or intercropping to accelerate SOM accumulation, while older stands might require interventions to mitigate aggregate breakdown through root properties. The study underscores the role of root systems in soil stability, suggesting that management practices promoting robust root development regardless of variety could enhance aggregate cohesion and long-term productivity.

Credit authorship contribution statement

WA: Writing - original draft, visualization, Investigation, Data curation, formal analysis. **AM** Investigation, Data curation. **TL:** visualization, formal analysis, **NK:** Writing – review & editing. **AS:** Writing – review & editing. **KS:** Investigation, formal analysis. **QY:** Investigation, Funding

acquisition, review & editing. **HY:** Writing – review & editing, **WL:** Investigation, Data curation.
WL: Validation, Supervision, Resources, Conceptualization, Funding acquisition.

Declaration of Competing Interest

The authors declare that they have no known competing financial interests or personal relationships that could have appeared to influence the work reported in this paper.

Data availability

Data will be made available on request.

Acknowledgment

This work was financially supported by the National Key Research and Development Program of China (2021YFD2200403-04), Hainan Province Postdoctoral Research Project (RZ2500001086) and the National Natural Science Foundation of China (No. 42367034 and 32160291).

References

Ali, W., Yang, M., Long, Q., Hussain, S., Chen, J., Clay, D., and He, Y.: Different fall/winter cover crop root patterns induce contrasting red soil (Ultisols) mechanical resistance through aggregate properties, *Plant and Soil*, 477, 461–474, <https://doi.org/10.1007/s11104-022-05430-4>, 2022.

Ali, W., Hussain, S., Chen, J., Hu, F., Liu, J., He, Y., and Yang, M.: Cover crop root-derived organic carbon influences aggregate stability through soil internal forces in a clayey red soil, *Geoderma*, 429, 116271, <https://doi.org/10.1016/j.geoderma.2022.116271>, 2023.

Barto, E. K., Alt, F., Oelmann, Y., Wilcke, W., and Rillig, M. C.: Contributions of biotic and abiotic factors to soil aggregation across a land use gradient, *Soil Biology and Biochemistry*, 42, 2316–2324, <https://doi.org/10.1016/j.soilbio.2010.09.008>, 2010.

Chen, C., Liu, W., Jiang, X., and Wu, J.: Effects of rubber-based agroforestry systems on soil

476 aggregation and associated soil organic carbon: Implications for land use, *Geoderma*, 299, 13–24,
 477 <https://doi.org/10.1016/j.geoderma.2017.03.021>, 2017.

478 Chen, J., Wu, Z., Zhao, T., Yang, H., Long, Q., and He, Y.: Rotation crop root performance and
 479 its effect on soil hydraulic properties in a clayey Utisol, *Soil and Tillage Research*, 213, 105136,
 480 <https://doi.org/10.1016/j.still.2021.105136>, 2021.

481 Deviren Saygin, S., Ari, F., Temiz, Ç., Arslan, Ş., Ünal, M. A., and Erpul, G.: Analysis of soil
 482 cohesion by fluidized bed methodology using integrable differential pressure sensors for a wide
 483 range of soil textures, *Computers and Electronics in Agriculture*, 191,
 484 <https://doi.org/10.1016/j.compag.2021.106525>, 2021.

485 Elliott, E. T.: Aggregate Structure and Carbon, Nitrogen, and Phosphorus in Native and Cultivated
 486 Soils, *Soil Science Society of America Journal*, 50, 627–633,
 487 <https://doi.org/10.2136/sssaj1986.03615995005000030017x>, 1986.

488 Forster, M., Ugarte, C., Lamandé, M., and Faucon, M.-P.: Root traits of crop species contributing
 489 to soil shear strength, *Geoderma*, 409, 115642, <https://doi.org/10.1016/j.geoderma.2021.115642>,
 490 2022.

491 Halder, M., Liu, S., Zhang, Z. B., Guo, Z. C., and Peng, X. H.: Effects of residue stoichiometric,
 492 biochemical and C functional features on soil aggregation during decomposition of eleven organic
 493 residues, *CATENA*, 202, 105288, <https://doi.org/10.1016/j.catena.2021.105288>, 2021.

494 He, Y., Yang, M., Huang, R., Wang, Y., and Ali, W.: Soil organic matter and clay zeta potential
 495 influence aggregation of a clayey red soil (Ultisol) under long-term fertilization, *Scientific Reports*,
 496 11, 20498, <https://doi.org/10.1038/s41598-021-99769-w>, 2021.

497 He, Y., Wu, Z., Zhao, T., Yang, H., Ali, W., and Chen, J.: Different plant species exhibit
 498 contrasting root traits and penetration to variation in soil bulk density of clayey red soil, *Agronomy*

Journal, 114, 867–877, <https://doi.org/10.1002/agj2.20972>, 2022.

Hok, L., de Moraes Sá, J. C., Boulakia, S., Reyes, M., de Oliveira Ferreira, A., Elie Tivet, F., Saab, S., Auccaise, R., Massao Inagaki, T., Schimiguel, R., Aparecida Ferreira, L., Briedis, C., Santos Canalli, L. B., Kong, R., and Leng, V.: Dynamics of soil aggregate-associated organic carbon based on diversity and high biomass-C input under conservation agriculture in a savanna ecosystem in Cambodia, CATENA, 198, 105065, <https://doi.org/10.1016/j.catena.2020.105065>, 2021.

Huang, M., Sun, S., Feng, K., Lin, M., Shuai, F., Zhang, Y., Lin, J., Ge, H., Jiang, F., and Huang, Y.: Effects of *Neyraudia reynaudiana* roots on the soil shear strength of collapsing wall in Benggang, southeast China, Catena, 210, 105883, <https://doi.org/10.1016/j.catena.2021.105883>, 2022.

Kaiser, M. and Asefaw Berhe, A.: How does sonication affect the mineral and organic constituents of soil aggregates? - A review, Journal of Plant Nutrition and Soil Science, 177, 479–495, <https://doi.org/10.1002/jpln.201300339>, 2014.

Kamau, S., Barrios, E., Karanja, N. K., Ayuke, F. O., and Lehmann, J.: Dominant tree species and earthworms affect soil aggregation and carbon content along a soil degradation gradient in an agricultural landscape, Geoderma, 359, 113983, <https://doi.org/10.1016/j.geoderma.2019.113983>, 2020.

Kemper, W. D. and Rosenau, R. C.: Aggregate Stability and Size Distribution, in: Agronomy Monograph, vol. 9, 425–442, <https://doi.org/10.2136/sssabookser5.1.2ed.c17>, 2018.

Kumar, A., Dorodnikov, M., Splettstößer, T., Kuzyakov, Y., and Pausch, J.: Effects of maize roots on aggregate stability and enzyme activities in soil, Geoderma, 306, 50–57, <https://doi.org/10.1016/j.geoderma.2017.07.007>, 2017.

522 Kurmi, B., Nath, A. J., Lal, R., and Das, A. K.: Water stable aggregates and the associated active
 523 and recalcitrant carbon in soil under rubber plantation, *Science of the Total Environment*, 703,
 524 135498, <https://doi.org/10.1016/j.scitotenv.2019.135498>, 2020.

525 Li, T., Hong, X., Liu, S., Wu, X., Fu, S., Liang, Y., Li, J., Li, R., Zhang, C., Song, X., Zhao, H.,
 526 Wang, D., Zhao, F., Ruan, Y., and Ju, X.: Cropland degradation and nutrient overload on Hainan
 527 Island: A review and synthesis, *Environmental Pollution*, 313, 120100,
 528 <https://doi.org/10.1016/j.envpol.2022.120100>, 2022.

529 Liao, J., Yang, X., Dou, Y., Wang, B., Xue, Z., Sun, H., Yang, Y., and An, S.: Divergent
 530 contribution of particulate and mineral-associated organic matter to soil carbon in grassland,
 531 *Journal of Environmental Management*, 344, 118536,
 532 <https://doi.org/10.1016/j.jenvman.2023.118536>, 2023.

533 Melo, T. R. de, Figueiredo, A., and Filho, J. T.: Clay behavior following macroaggregate
 534 breakdown in Ferralsols, *Soil and Tillage Research*, 207, 104862,
 535 <https://doi.org/10.1016/j.still.2020.104862>, 2021.

536 Nornadiah Mohd Razali Yap Bee Wah: Power comparisons of Shapiro-Wilk, Kolmogorov-
 537 Smirnov, Lilliefors and Anderson-Darling tests, *Journal of Statistical Modeling and Analytics*, 21–
 538 33, 2011.

539 Oleghe, E., Naveed, M., Baggs, E. M., and Hallett, P. D.: Plant exudates improve the mechanical
 540 conditions for root penetration through compacted soils, *Plant and Soil*, 421, 19–30,
 541 <https://doi.org/10.1007/s11104-017-3424-5>, 2017.

542 Perović, V., Kadović, R., Đurđević, V., Pavlović, D., Pavlović, M., Čakmak, D., Mitrović, M., and
 543 Pavlović, P.: Major drivers of land degradation risk in Western Serbia: Current trends and future
 544 scenarios, *Ecological Indicators*, 123, 107377, <https://doi.org/10.1016/j.ecolind.2021.107377>,

2021.

Poirier, V., Roumet, C., Angers, D. A., and Munson, A. D.: Species and root traits impact macroaggregation in the rhizospheric soil of a Mediterranean common garden experiment, *Plant and Soil*, 424, 289–302, <https://doi.org/10.1007/s11104-017-3407-6>, 2018a.

Poirier, V., Roumet, C., and Munson, A. D.: The root of the matter: Linking root traits and soil organic matter stabilization processes, *Soil Biology and Biochemistry*, 120, 246–259, <https://doi.org/10.1016/j.soilbio.2018.02.016>, 2018b.

Prăvălie, R., Nita, I.-A., Patriche, C., Niculiță, M., Birsan, M.-V., Roșca, B., and Bandoc, G.: Global changes in soil organic carbon and implications for land degradation neutrality and climate stability, *Environmental Research*, 201, 111580, <https://doi.org/10.1016/j.envres.2021.111580>, 2021.

Rabot, E., Wiesmeier, M., Schlüter, S., and Vogel, H.-J.: Soil structure as an indicator of soil functions: A review, *Geoderma*, 314, 122–137, <https://doi.org/10.1016/j.geoderma.2017.11.009>, 2018.

Rossi, L. M. W., Mao, Z., Merino-Martín, L., Roumet, C., Fort, F., Taugourdeau, O., Boukcim, H., Fourtier, S., Del Rey-Granado, M., Chevallier, T., Cardinael, R., Fromin, N., and Stokes, A.: Pathways to persistence: plant root traits alter carbon accumulation in different soil carbon pools, *Plant and Soil*, 452, 457–478, <https://doi.org/10.1007/s11104-020-04469-5>, 2020.

Schad, P.: World Reference Base for Soil Resources—Its fourth edition and its history, *Journal of Plant Nutrition and Soil Science*, 186, 151–163, <https://doi.org/10.1002/jpln.202200417>, 2023.

Shao, W., Zhang, Z., Guan, Q., Yan, Y., and Zhang, J.: Comprehensive assessment of land degradation in the arid and semiarid area based on the optimal land degradation index model, *CATENA*, 234, 107563, <https://doi.org/10.1016/j.catena.2023.107563>, 2024.

568 Shen, N., Wang, Z., Guo, Q., Zhang, Q., Wu, B., Liu, J., Ma, C., Delang, C. O., and Zhang, F.:
 569 Soil detachment capacity by rill flow for five typical loess soils on the Loess Plateau of China,
 570 Soil and Tillage Research, 213, 105159, <https://doi.org/10.1016/j.still.2021.105159>, 2021.

571 Smith, D. J., Wynn-Thompson, T. M., Williams, M. A., and Seiler, J. R.: Do roots bind soil?
 572 Comparing the physical and biological role of plant roots in fluvial streambank erosion: A mini-
 573 JET study, Geomorphology, 375, 107523, <https://doi.org/10.1016/j.geomorph.2020.107523>, 2021.

574 Sun, R., Wu, Z., Lan, G., Yang, C., and Fraedrich, K.: Effects of rubber plantations on soil
 575 physicochemical properties on Hainan Island, China, Journal of Environmental Quality, 50, 1351–
 576 1363, <https://doi.org/10.1002/jeq2.20282>, 2021.

577 Sun, R., Lan, G., Yang, C., Wu, Z., Chen, B., and Fraedrich, K.: Soil quality variation and its
 578 driving factors within tropical forests on Hainan Island, China, Land Degradation and
 579 Development, 34, 3418–3432, <https://doi.org/10.1002/ldr.4693>, 2023.

580 Team, R. C.: a Language and Environment for Statistical Computing, 2017.

581 Thomas, A., Bentley, L., Feeney, C., Lofts, S., Robb, C., Rowe, E. C., Thomson, A., Warren-
 582 Thomas, E., and Emmett, B.: Land degradation neutrality: Testing the indicator in a temperate
 583 agricultural landscape, Journal of Environmental Management, 346, 118884,
 584 <https://doi.org/10.1016/j.jenvman.2023.118884>, 2023.

585 Vannoppen, W., Vanmaercke, M., De Baets, S., and Poesen, J.: A review of the mechanical effects
 586 of plant roots on concentrated flow erosion rates, Earth-Science Reviews, 150, 666–678,
 587 <https://doi.org/10.1016/j.earscirev.2015.08.011>, 2015.

588 Vannoppen, W., De Baets, S., Keeble, J., Dong, Y., and Poesen, J.: How do root and soil
 589 characteristics affect the erosion-reducing potential of plant species?, Ecological Engineering, 109,
 590 186–195, <https://doi.org/10.1016/j.ecoleng.2017.08.001>, 2017.

591 Walkley, A. and Black, I. A.: An examination of the degtjareff method for determining soil organic
 592 matter, and a proposed modification of the chromic acid titration method, *Soil Science*, 37, 29–38,
 593 <https://doi.org/10.1097/00010694-193401000-00003>, 1934.

594 Wang, B., Zhang, G.-H., Yang, Y.-F., Li, P.-P., and Liu, J.-X.: Response of soil detachment
 595 capacity to plant root and soil properties in typical grasslands on the Loess Plateau, *Agriculture,*
 596 *Ecosystems & Environment*, 266, 68–75, <https://doi.org/10.1016/j.agee.2018.07.016>, 2018a.

597 Wang, B., Zhang, G.-H., Yang, Y.-F., Li, P.-P., and Liu, J.-X.: The effects of varied soil properties
 598 induced by natural grassland succession on the process of soil detachment, *CATENA*, 166, 192–
 599 199, <https://doi.org/10.1016/j.catena.2018.04.007>, 2018b.

600 Wang, G., Huang, Y., Li, R., Chang, J., and Fu, J.: Influence of Vetiver Root System on
 601 Mechanical Performance of Expansive Soil: Experimental Studies, *Advances in Civil Engineering*,
 602 2020, 1–11, <https://doi.org/10.1155/2020/2027172>, 2020a.

603 Wang, G. Y., Huang, Y. G., Li, R. F., Chang, J. M., and Fu, J. L.: Influence of vetiver root on
 604 strength of expansive soil-experimental study, *PLoS ONE*, 15, 1–20,
 605 <https://doi.org/10.1371/journal.pone.0244818>, 2020b.

606 Wang, J., Wei, H., Huang, J., He, T., and Deng, Y.: Soil aggregate stability and its response to
 607 overland runoff–sediment transport in karst peak–cluster depressions, *Journal of Hydrology*, 620,
 608 129437, <https://doi.org/10.1016/j.jhydrol.2023.129437>, 2023.

609 Wuddivira, M. N., Stone, R. J., and Ekwue, E. I.: Clay, Organic Matter, and Wetting Effects on
 610 Splash Detachment and Aggregate Breakdown under Intense Rainfall, *Soil Science Society of*
 611 *America Journal*, 73, 226–232, <https://doi.org/10.2136/sssaj2008.0053>, 2009.

612 Wuddivira, M. N., Stone, R. J., and Ekwue, E. I.: Influence of cohesive and disruptive forces on
 613 strength and erodibility of tropical soils, *Soil and Tillage Research*, 133, 40–48,

614 <https://doi.org/10.1016/j.still.2013.05.012>, 2013.

615 Xu, W., Liu, W., Tang, S., Yang, Q., Meng, L., Wu, Y., Wang, J., Wu, L., Wu, M., Xue, X., Wang,
616 W., and Luo, W.: Long-term partial substitution of chemical nitrogen fertilizer with organic
617 fertilizers increased SOC stability by mediating soil C mineralization and enzyme activities in a
618 rubber plantation of Hainan Island, China, *Applied Soil Ecology*, 182, 104691,
619 <https://doi.org/10.1016/j.apsoil.2022.104691>, 2023.

620 Yang, Q., Li, J., Xu, W., Wang, J., Jiang, Y., Ali, W., and Liu, W.: Substitution of Inorganic
621 Fertilizer with Organic Fertilizer Influences Soil Carbon and Nitrogen Content and Enzyme
622 Activity under Rubber Plantation, *Forests*, 15, 756, <https://doi.org/10.3390/f15050756>, 2024.

623 Yu, Z., Zheng, Y., Zhang, J., Zhang, C., Ma, D., Chen, L., and Cai, T.: Importance of soil
624 interparticle forces and organic matter for aggregate stability in a temperate soil and a subtropical
625 soil, *Geoderma*, 362, 114088, <https://doi.org/10.1016/j.geoderma.2019.114088>, 2020.

626 Yudina, A. and Kuzyakov, Y.: Dual nature of soil structure: The unity of aggregates and pores,
627 *Geoderma*, 434, 116478, <https://doi.org/10.1016/j.geoderma.2023.116478>, 2023.

628 Zhang, C.-B., Chen, L.-H., and Jiang, J.: Why fine tree roots are stronger than thicker roots: The
629 role of cellulose and lignin in relation to slope stability, *Geomorphology*, 206, 196–202,
630 <https://doi.org/10.1016/j.geomorph.2013.09.024>, 2014.

631 Zhu, X., Liu, W., Yuan, X., Chen, C., Zhu, K., Zhang, W., and Yang, B.: Aggregate stability and
632 size distribution regulate rainsplash erosion: Evidence from a humid tropical soil under different
633 land-use regimes, *Geoderma*, 420, 115880, <https://doi.org/10.1016/j.geoderma.2022.115880>,
634 2022.

635 Zou, X., Zhu, X., Zhu, P., Singh, A. K., Zakari, S., Yang, B., Chen, C., and Liu, W.: Soil quality
636 assessment of different *Hevea brasiliensis* plantations in tropical China, *Journal of Environmental*

Management, 285, 112147, <https://doi.org/10.1016/j.jenvman.2021.112147>, 2021.

Table captions

Table. 1. Basic physical and chemical characteristics of the experimental site.

Treatments	Soil depth (cm)	pH	BD (g/cm ³)	TOP (%)	SMC (%)	SOM (g/kg)	AN (mg/kg)	AP (mg/kg)	AK (mg/kg)
CK	0 -20	4.17	1.52	26.37	17.46	12.34	11.92	1.69	24.42
	20 - 40	4.21	1.56	23.26	15.25	11.36	11.45	1.56	18.15
5Y_RF	0 -20	4.37	1.39	28.39	19.25	20.98	11.63	2.79	34.62
	20 - 40	4.13	1.52	23.01	17.63	16.30	10.67	1.73	17.97
11Y_RF	0 -20	3.89	1.43	24.81	21.67	22.68	11.84	2.31	25.23
	20 - 40	4.02	1.51	23.1	20.77	20.56	10.42	1.7	16.44
20Y_RF	0 -20	4.08	1.36	24.98	21.41	23.37	10.67	2.33	29.02
	20 - 40	4.22	1.43	20.31	20.2	21.16	10.39	1.99	23.12
27Y_RF	0 -20	4.08	1.32	25.05	23.68	21.78	11.77	2.39	25.83
	20 - 40	4.26	1.41	25.24	19.9	21.04	10.17	1.84	18.92
MF	0 -20	4.42	1.31	29.52	22.76	21.20	13.47	1.81	36.15
	20 - 40	4.35	1.39	26.58	20.11	20.29	12.84	1.33	19.94

Note: BD: Bulk density; TOP: Total porosity; SMC: Soil moisture content; SOM: Soil organic matter; AN: Available nitrogen; AP: Available phosphorus; AK: Available potassium.

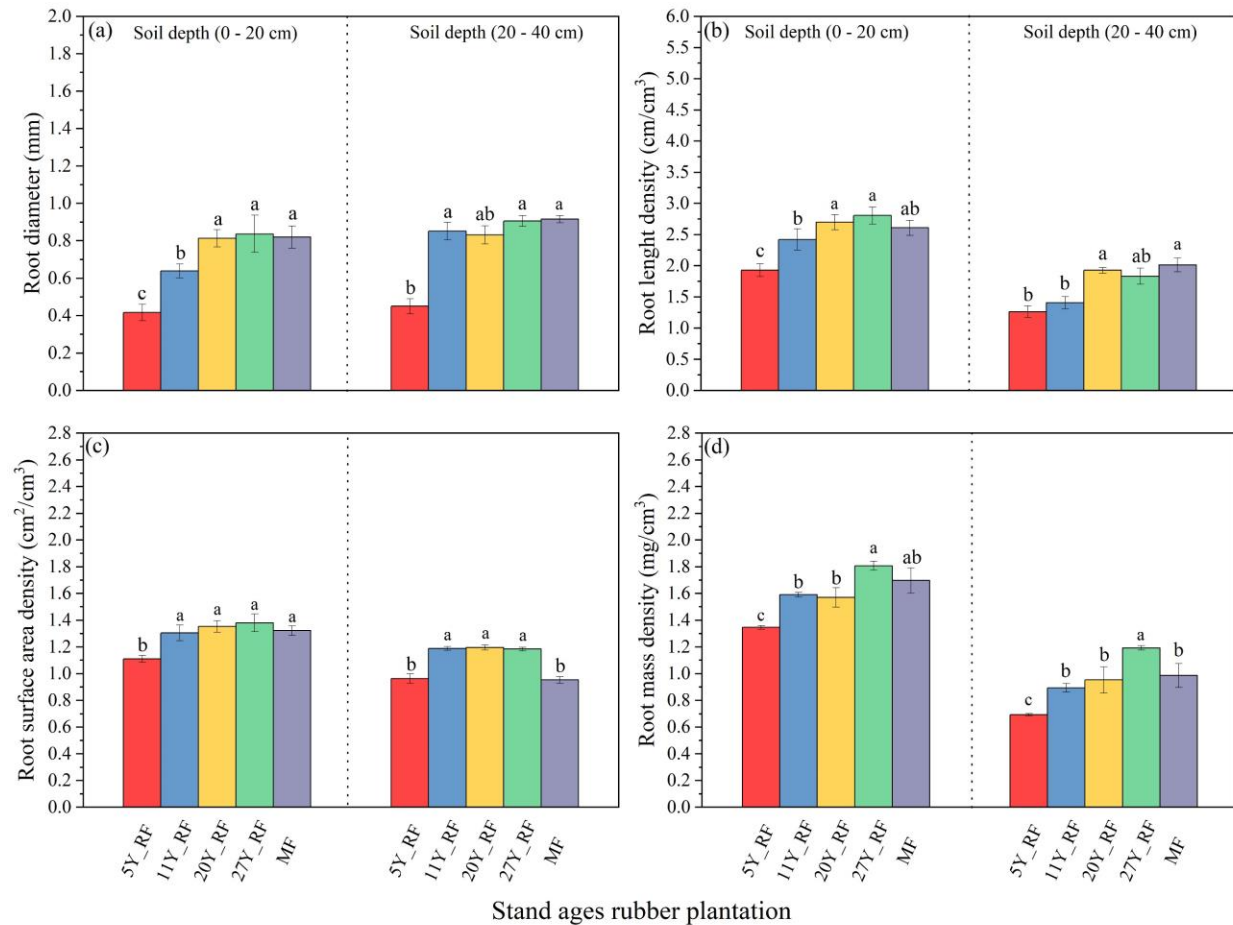


Figure 1. Different stand-age rubber plantation root morphological properties with soil depths. Each treatment was replicated three times ($n = 3$), and results are presented as mean \pm standard deviation. (a) Root diameter (RD), (b) Root length density (RLD), (c) Root surface area density (RSD), and (d) Root mass density (RMD).

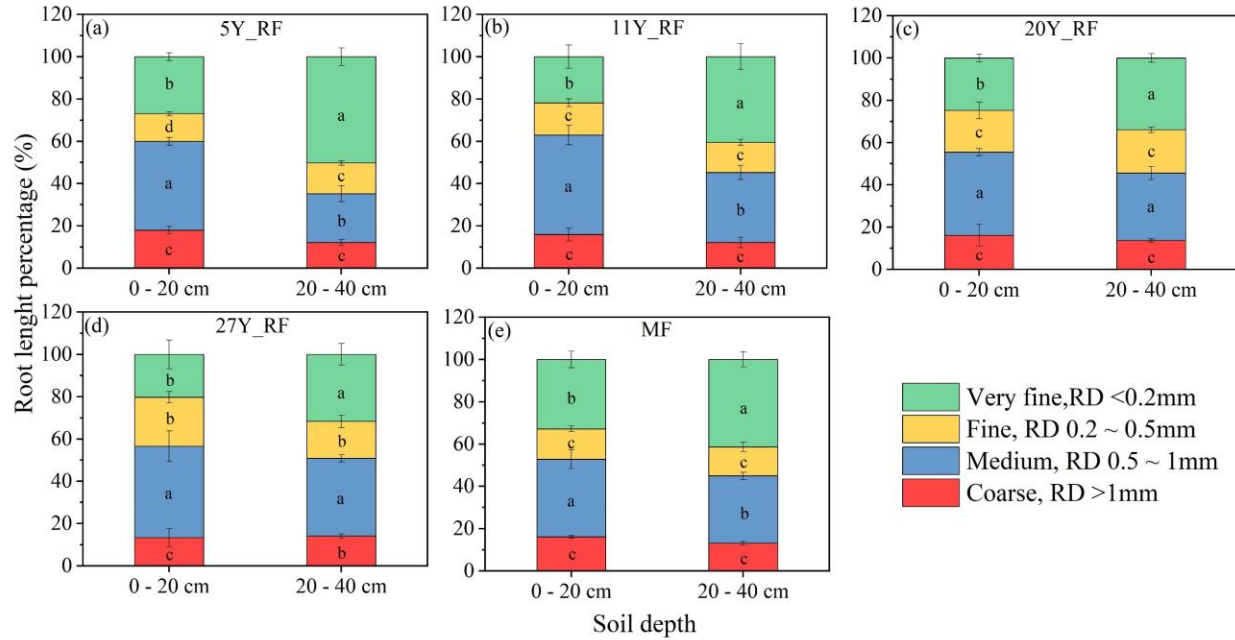


Figure 2. Root diameter distribution of rubber plants at different stand ages represented by the root length percentage across four class diameters. Each treatment was replicated three times ($n = 3$), and results are presented as mean \pm standard deviation

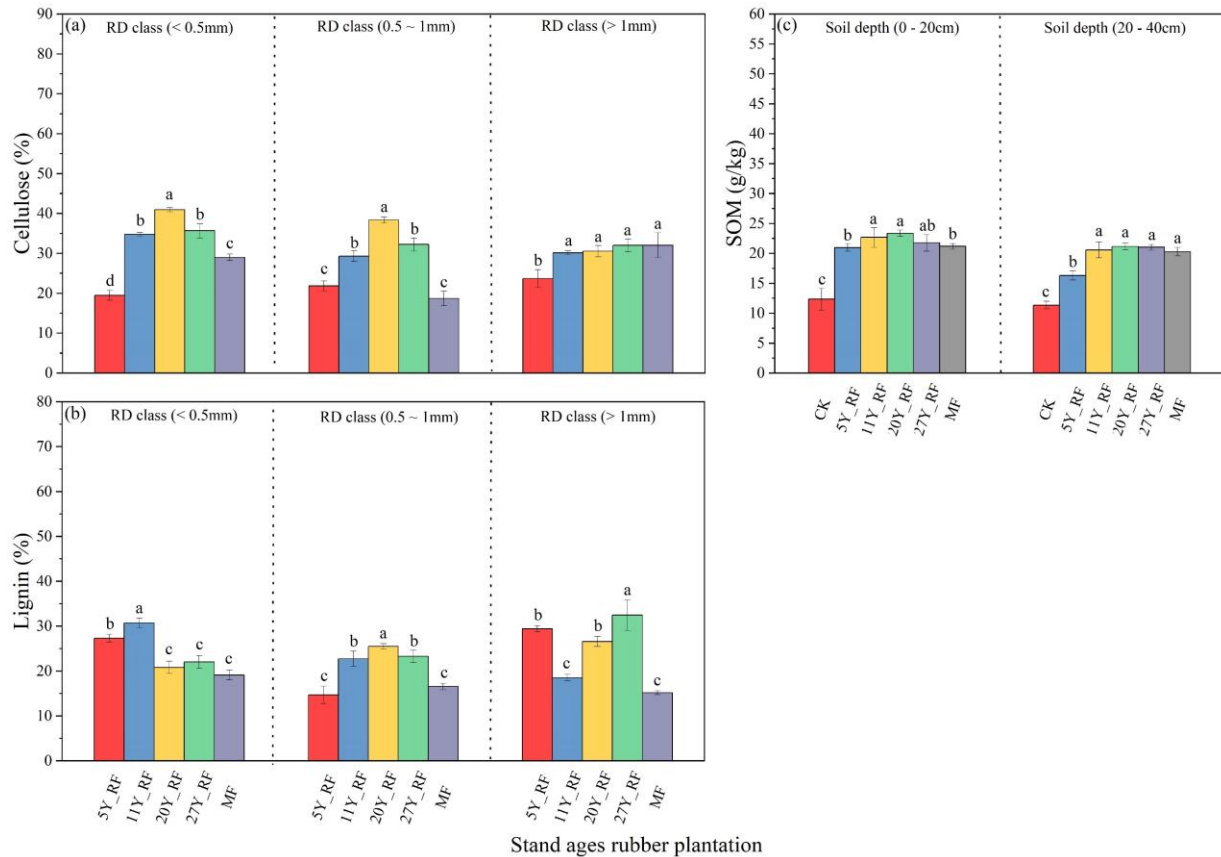


Figure 3. Different stand-age rubber plantation root chemical compositions and soil organic matter (SOM) distributions. Each treatment was replicated three times ($n = 3$), and results are presented as mean \pm standard deviation. (a) Cellulose, (b) Lignin, and (c) Soil organic matter (SOM).

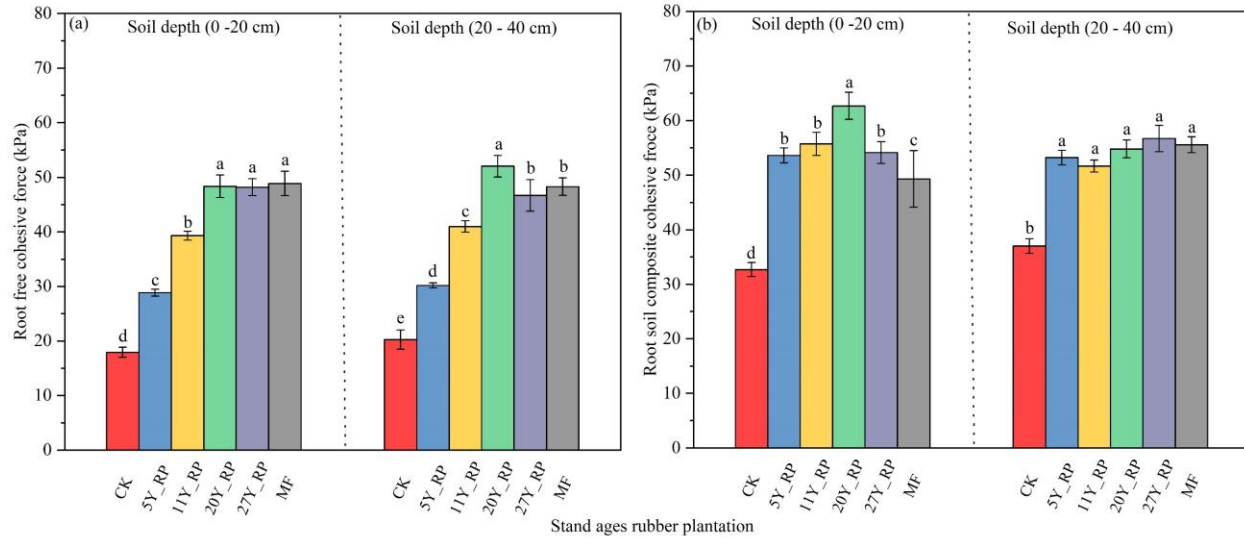


Figure 4. Soil cohesive force distribution under different stand-age rubber plantations. Each treatment was replicated three times ($n = 3$), and results are presented as mean \pm standard deviation (a) Root-free cohesive force (RFCS), (b) Root-soil composite cohesive force (RSCCF).

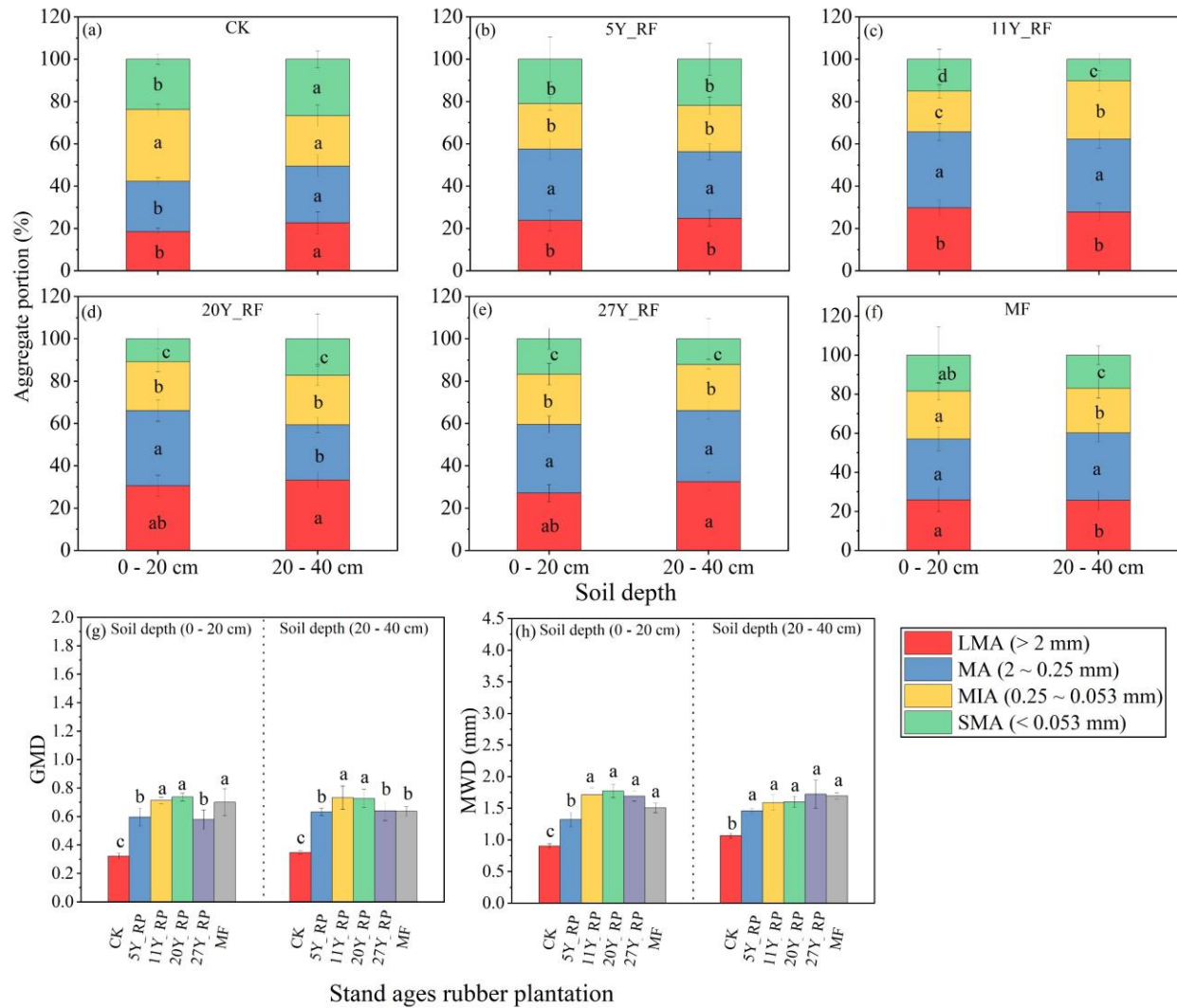


Figure 5. Different stand-age rubber plantation aggregate size distributions and soil aggregate stabilities (MWD and GWD) with soil depths. Each treatment was replicated three times ($n = 3$), and results are presented as mean \pm standard deviation.

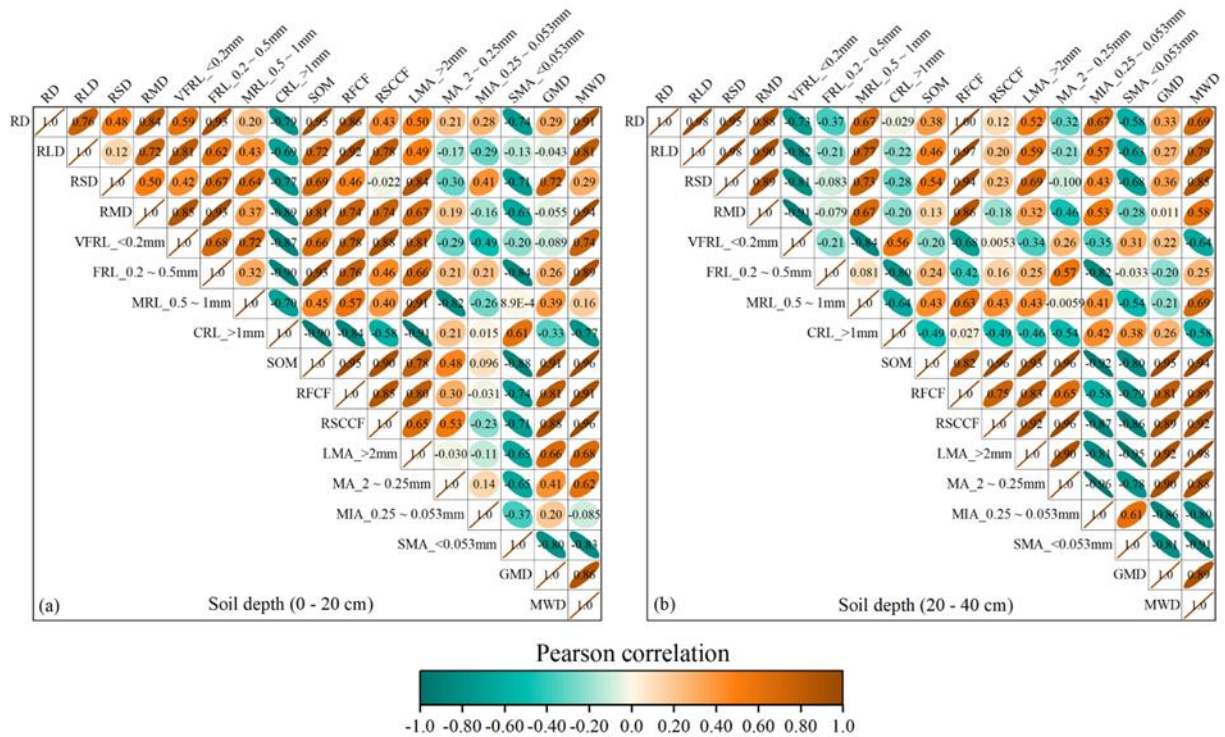


Figure 6. Pearson correlations ($P < 0.05$) for all root traits, aggregate stabilities, soil organic matter, and soil cohesive forces. RD: root diameter; RLD: root length density; RSD: root surface area density; RMD: root mass density; VFRL: very fine root length; FRL: fine root length; MRL: medium root length; CRL: coarse root length; SOM: soil organic matter; RFCF: root-free cohesive force; RSCCF: root–soil composite cohesive force; LMA: large macroaggregates (> 2 mm); MA: macroaggregates (2–0.25 mm); MIA: microaggregates (0.25–0.053 mm); SMA: small microaggregates (< 0.053 mm); GMD: geometric mean diameter; MWD: mean weight diameter. The dark brown color indicates a positive correlation, and the pine green color indicates a negative correlation.

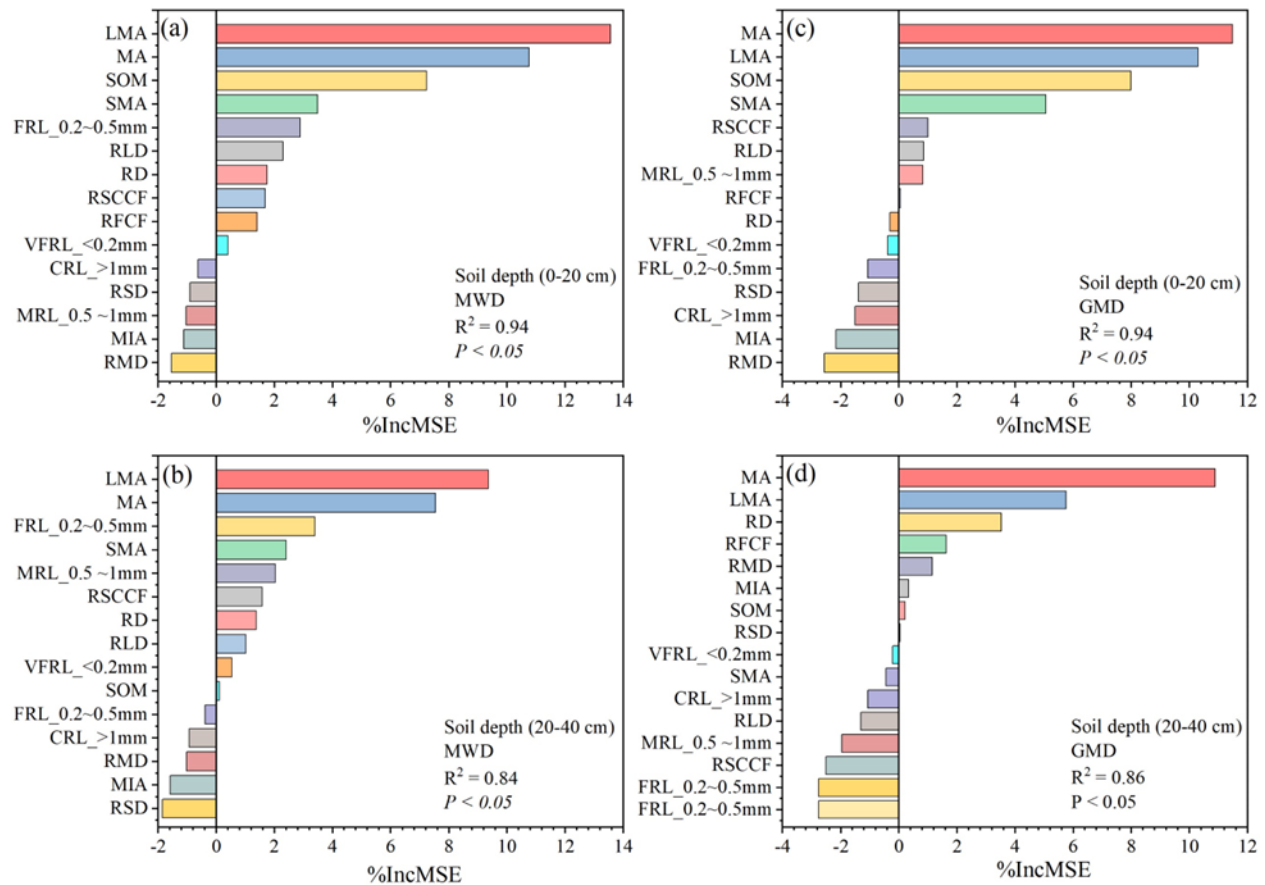


Figure 7. Random forest model ($P < 0.05$) to identify the key predictors of mean weight diameter (MWD) and geometric mean diameter (GMD). RD: root diameter; RLD: root length density; RSD: root surface area density; RMD: root mass density; VFRL: very fine root length; FRL: fine root length; MRL: medium root length; CRL: coarse root length; SOM: soil organic matter; RFCF root-free cohesive force; RSCCF: root-soil composite cohesive force; LMA: large macroaggregates (> 2 mm); MA: macroaggregates (2–0.25 mm); MIA: microaggregates (0.25–0.053 mm); SMA: small microaggregates (< 0.053 mm).

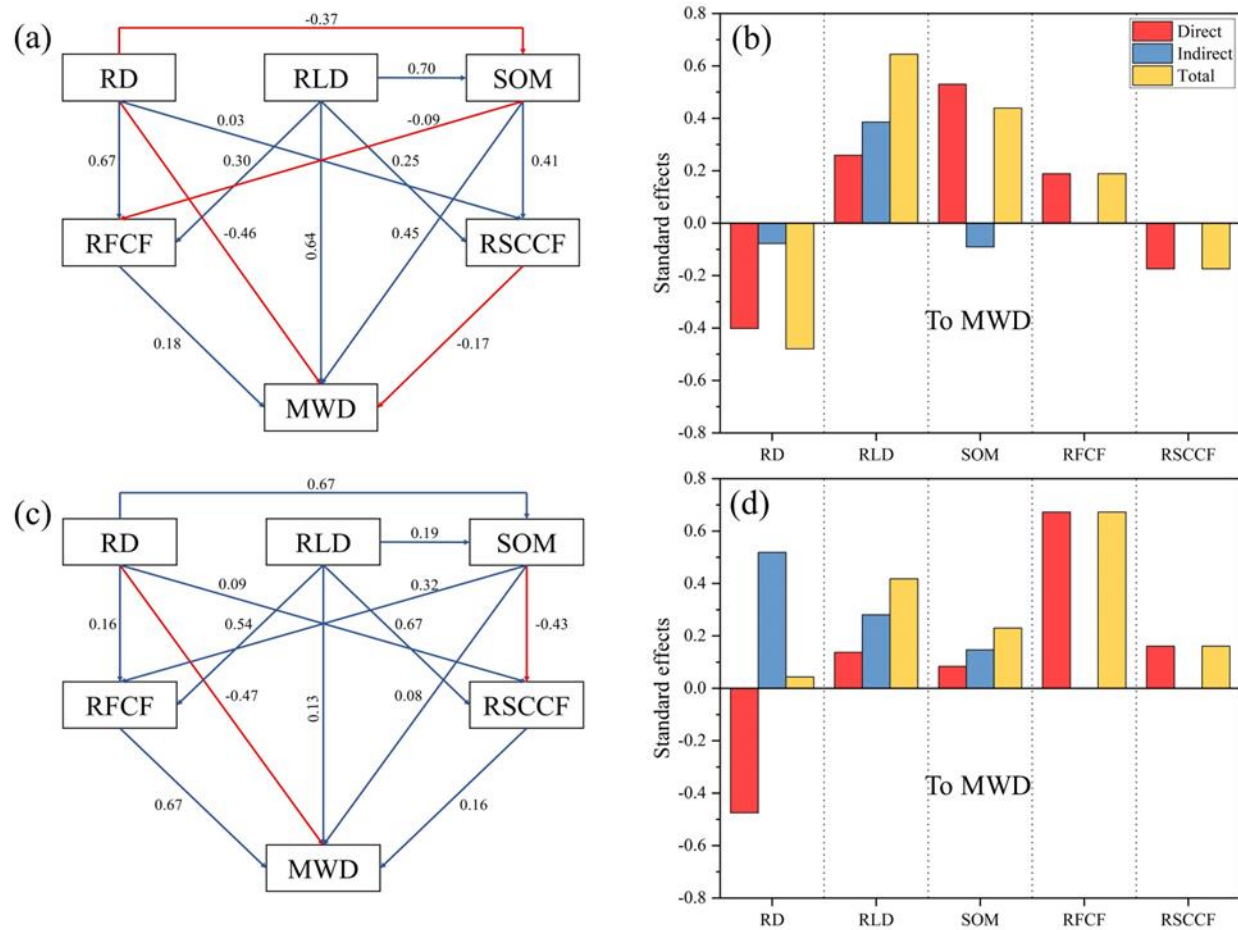


Figure 8. Partial least squares-path models (PLS-PM) ($P < 0.05$) indicating the indirect and direct impact of root properties, soil organic matter, and cohesive forces on soil aggregate stability at 0–20 cm (a, and b) and 20–40 cm (c, and d). The numbers near the arrows are standardized path coefficients. The blue line indicates the positive direction, and the red line indicates the negative direction. RD: root diameter; RLD: root length density; SOM: soil organic matter; RFCF: root-free cohesive force; RSCCF: root-soil composite cohesive force; MWD: mean weight diameter.